Research & Reviews: Journal of Material Sciences e-ISSN: 2321-6212

Layered/Spinel Heterostructured Li-Rich Cathode Materials without Oxygen Loss in Lithium-ion Battery

Shan Xu[1,2]*, Jingcheng Xu[3]

[1]Hubei Wisdom Comprehensive Energy Industry Technology Research, Wuhan, China

[2]Division of Fuel Cell and Battery, Dalian National Laboratory for Clean Energy, Dalian Institute of Chemical Physics, Chinese Academy of Sciences, Dalian, China

[3]Wuhan Guide Infrared, Wuhan, China

Research Article

Received: 29-May-2024, Manuscript No. JOMS-24-137603; **Editor assigned:** 03-Jun-2024, PreQC No. JOMS-24-137603 (PQ); **Reviewed:** 17-Jun-2024, QC No. JOMS-24-137603; **Revised:** 24-Jun-2024, Manuscript No. JOMS-24-137603 (R); **Published:** 01-Jul-2024, DOI: 10.4172/2321-6212.12.2.003

***For Correspondence:** Shan Xu, Hubei Wisdom Comprehensive Energy Industry Technology Research, Wuhan, China

E-mail: 1[illegible]88214[illegible]@qq.com

Citation: Xu S, et al. Layered/Spinel Heterostructured Li-Rich Cathode Materials without Oxygen Loss in Lithium-ion Battery. RRJ Mater Sci. 2024;12:003.

ABSTRACT

Abstract Lithium-excess manganese layered oxides, which are commonly described by the chemical formula $xLiMnO_3 \cdot (1-x)\ LiMO_2$ (M=Co, Ni, Mn, etc.), are of great importance as cathode materials for rechargeable lithium batteries. A mechanism involving simultaneous Li and O removal is often proposed. Oxygen loss and MnO_2 formation appear when first charging across a voltage plateau at 4.5 V *vs* Li/Li^+, which is bottleneck of industrialization for the resulting security problems. In our recent findings, layered/spinel hetero structured Li-rich material $Li_{1.2}Ni_{0.2}Mn_{0.6}O_2$ consist of Li_2MnO_3, $LiNiMnO_2$ and $LiNi_{0.5}Mn_{1.5}O_4$ without oxygen loss was desired. After assembling it into lithium-ion battery, CV curves have no oxygen evolution peak and no oxygen appears *in situ* Differential Electrochemical Mass Spectrometry (DEMS). According to the first principle, Li^+ ions in Li_2MnO_3 de-intercalate then Ni^{2+} ions of $LiNi_{0.5}Mn_{1.5}O_4$ migrate into the sites when first charging, which avoids the oxygen loss from the collapse of Li_2MnO_3. The exist of spinel phase make the phase transition process of circulation stable, which contributed to the high cycling performance for lithium-ion battery (300 and 220 mAh g^{-1} after 200th cycles at 0.1 and 0.5C-rate (1C=250 mA g^{-1}).

Keywords: Li-rich; Cathode materials; Oxygen loss high capacity; Lithium-ion batteries.

INTRODUCTION

As the new energy industry booms, Lithium-Ion Batteries (LIBs) with higher energy and power densities as the leading role of battery industry is applied to 3C, energy storage and many other fields such as Hybrid Electric Vehicles (HEVs) and Electric Vehicles (EVs).

Layered structure Li-rich materials xLi_2MnO_3 (1−x) $LiMO_2$ (M = Mn, Ni, and Co) (LMR) are more and more attractive to researchers because of its high theoretical specific capacity (350 mAh g^{-1}) and high discharge voltage (4.5 V). However, the materials also suffer from some disadvantages with initially large capacity loss and poor rate cycling performance [1-7]. As reporters' views, oxygen loss is the main reason for its poor stability [8, 9]. It is generally believed that the charging process of the materials is divided into two stages. When the charge voltage *vs* Li/Li^+ below to 4.5 V, the capacity is mainly provided by $LiMO_2$ component. After charged to 4.5 V, there is a long plateau accompanied with a net loss of Li_2O from the Li_2MnO_3 component [10]. The net loss of Li_2O leads to a huge irreversible capacity loss in the initial cycle [10,11]. Meanwhile, some oxygen extracted from the lattice results in the transition metal ions migration leading to phase transformation to spinel structure [10,12-17]. The cyclic stability of the material is reduced rapidly due to the structural failure, which is the main factor in its inability to enter the market.

Layered/Spinel Hetero-structured (LSH) Li-rich materials is a new type of material that relieves voltage attenuation of LMR proposed by Su etc. [18] for the first time in 2013, which was improved successively by researchers in recent years [19-29]. Spinel structure was brought in to lower the initial irreversible capacity and maintain the phase transition stable. Spinel coating is preferred by researchers attributed to the consistency with phase transition [30-37]. So far, the coating methods include from simple sol-gel, co-precipitation to complicated as Atomic Layer Deposition (ALD), Thermal Evaporation (TE) Pulsed Laser Deposition (PLD) and reactive magnetron sputtering (RMS) [37-49]. These methods are all adding a coating process after preparing LMR, some of them are difficult to industrialize. What's more, it did not fundamentally solve the problem of oxygen loss.

This study presents a concept to obtain LSH without oxygen loss. Firstly, hydrothermal method was used to obtain the uniform-sized microspheres of $Ni_{0.2}Mn_{0.6}CO_3$. With annealing at the appropriate temperature, spinel structure material $LiNi_{0.5}Mn_{1.5}O_4$ was formed with $LiMO_2$. It is worth mentioning that the nickel ions in spinel phase play a fatal role in the process without oxygen loss. In the process of charging, lithium ions of Li-Mn layer off from Li_2MnO_3, nickel ions from spinel phase move into the above lithium vacancy, directly transformed Li_2MnO_3 into $LiMO_2$, which not only has no collapse of Li_2MnO_3 structure and oxygen loss, but also enhance the capacity attributed to the high theoretical specific capacity of $LiMO_2$. In order to explain the reaction mechanism of the material and its corresponding changes of crystal structure, composition and electrochemical process more specifically, various properties involving morphological, structural, and electrochemical performances of as-prepared material $Li_{1.2}Ni_{0.2}Mn_{0.6}O_2$ (LNMO) were evaluated and probed. The first principle was applied to the diffusion process of ions during charging.

MATERIALS and METHODS

Experimental details

$NiCO_3$ and $CoCO_3$ were mixed and ground at a ratio of 1:3, urea is used to regulate the pH value for hydrothermal reaction at 90°C for 24 hrs with ethanol as the solvent. $Ni_{0.2}Co_{0.6}CO_3$ was obtained after dehydration at 120°C, $Ni_{0.2}Co_{0.6}O_2$ was obtained after annealing at 450°C for 5 hrs. Li_2CO_3 and $Ni_{0.2}Co_{0.6}O_2$ were mixed and ground at a ratio of 3:2, $Li_{1.2}Ni_{0.2}Co_{0.6}O_2$ was obtained after annealing at 850°C for 12 hrs.

The structure and crystallinity of the samples were characterized using an X-ray diffractometer (XRD; Rigaku X-ray diffractometer) with Cu Kα radiation source (λ=0.1506 nm) under a voltage of 40 kV and a current of 30 mA. The morphology and elementary composition of the samples were observed by scanning electron microscopy (SEM; JEOL JSM, 65 10 V), transmission electron microscopy (TEM; JEM-2100, 200kV) and Energy-Dispersive Spectrometer (EDS). The chemical states of LNMO during the circulation were analyzed by X-ray photoelectron spectroscopy (XPS; Thermofisher ESCALAB 250Xi, 15kV, 10.8mA). Here, we demonstrate directly that there is no oxygen produced during charging to 4.8 V, by *in situ* differential electrochemical mass spectrometry (DEMS; HIDEN HPR20, 70 eV, 900 V).

A mixture of 80% wt $Li_{1.2}Ni_{0.2}Mn_{0.6}O_2$, 10% wt. super p, and 10% wt. Polyvinylidene Fluoride (PVDF) dissolved in 1-methyl-2-pyrrolidone (NMP) was stirred to form a homogeneous slurry. The slurry was spread on an Al foil coated carbon to form an electrode sheet. The sheet was dried at 120℃ for 10 hrs in vacuum oven. Half-cells were assembled in an Ar-filled glove-box with 1 mol/L LiPF6/EC+DMC (1:1 in volume) as the electrolyte and metallic lithium foil as the counter electrode.

The Cyclic Voltammetry (CV) was measured by an electrochemical workstation (CHI660C) between 2 and 4.8 V at a scan rate of 0.3 mV s^{-1}. The Electrochemical Impedance Spectroscopy (EIS) measurements were performed with CHI760E over the frequency range of 0.01～100 kHz with an amplitude of 5 mV. Galvanostatic charge/discharge cycling for lithium-ion batteries was carried out in the range of 2.0~4.8 V at 0.1 and 0.5 C-rate (1C = 250 mA g^{-1}). The densities used for rate capability for lithium-ion batteries were from 0.1 to 10 C, and for solid-state lithium batteries were from 25 mA g^{-1} to 2500 mA g^{-1}.

RESULTS AND DISCUSSION

Material characterization

The synthesis of LNMO was achieved by a two-step procedure divided into hydrothermal and annealing methods shown in Scheme 1. Figure 2 (a, b) are the X-ray diffraction patterns of the precursor $Ni_{0.2}Mn_{0.6}CO_3$, $Ni_{0.2}Mn_{0.6}O_2$ and product $Li_{1.2}Ni_{0.2}Mn_{0.6}O_2$. The precursor before annealing is $Ni_{0.2}Mn_{0.6}CO_3$, whose diffraction peaks is consisting with $MnCO_3$ (a=b=4.790 Å, c=15.694 Å, space group R-3c (167), JCPDS NO.14-1472). The precursor after annealing is consist of $NiMnO_3$ (a=b=4.890 Å, c=13.1 Å, space group R-3 (148), JCPDS NO.48-1330) and Mn_2O_3 (a=9.416 Å, b=9.424 Å, c=9.405 Å, space group Pcab (61), JCPDS NO.24-0508). The characteristic diffraction peaks of layered Li-rich materials can be obviously in Figure and are well indexed to the α-$NaFeO_2$ layered structure with R-3 m symmetry except for weak superlattice reflections around 20-25° corresponding to a Li_2MnO_3 component with monoclinic structure (space group C/2m). More importantly, it presents the characteristic diffraction peaks at 36° and 38° respectively represent the lattice plane (311) and (222) of spinel structure $LiNi_{0.5}Mn_{1.5}O_4$. Know then, the sample is composed of three phases $LiMO_2$, Li_2MnO_3 and $LiNi_{0.5}Mn_{1.5}O_4$ accurately. SEM images of precursor $Ni_{0.2}Mn_{0.6}CO_3$, $Ni_{0.2}Mn_{0.6}O_2$ and product $Li_{1.2}Ni_{0.2}Mn_{0.6}O_2$ are present in Figure 2c. The diagram shows the $Ni_{0.2}Mn_{0.6}CO_3$ obtained by hydrothermal method as microspheres, and core-shell structure forms after early sintering due to the loss of CO_2. The product restores the microsphere, from whose elemental mapping the distribution of elements of Ni, Mn and O is seen, and there is no obvious difference of phase.

Figure 1. Schematic illustration on the formation process of rich-LI LNMO

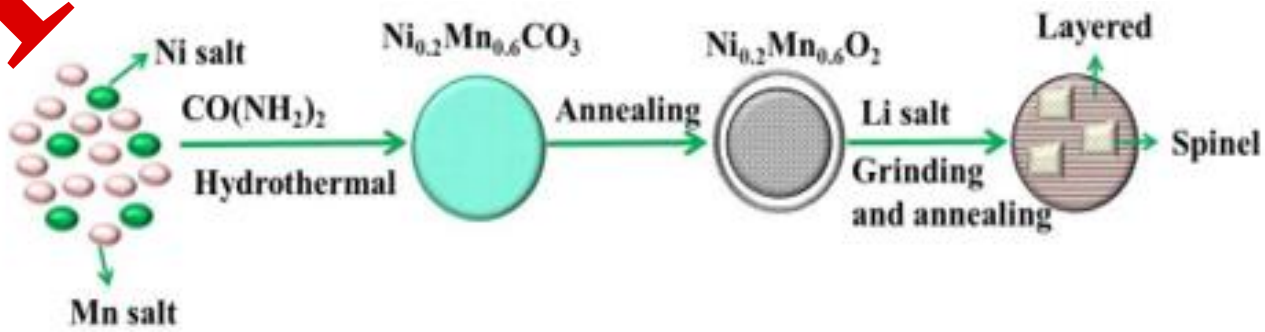

Figure 2. (a, b) XRD of precursor $Ni_{0.2}Mn_{0.6}CO_3$, $Ni_{0.2}Mn_{0.6}O_2$ and product $Li_{1.2}Ni_{0.2}Mn_{0.6}O_2$; (c) SEM images of above materials. Note: (a) R-3 $NiMnO_3$; Pcab Mn_2O_3, (b) (•) R-3m, (•) C2/C.

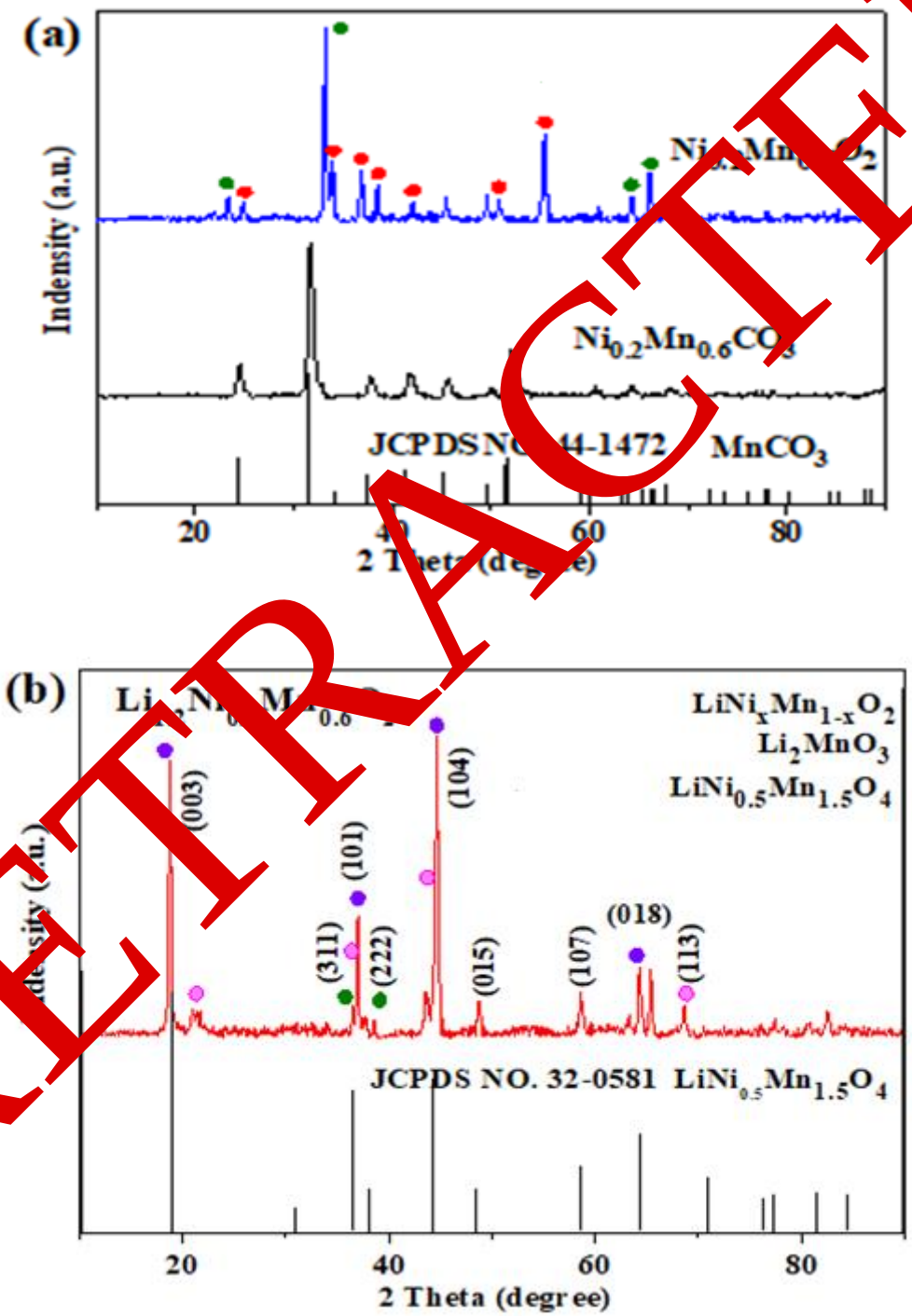

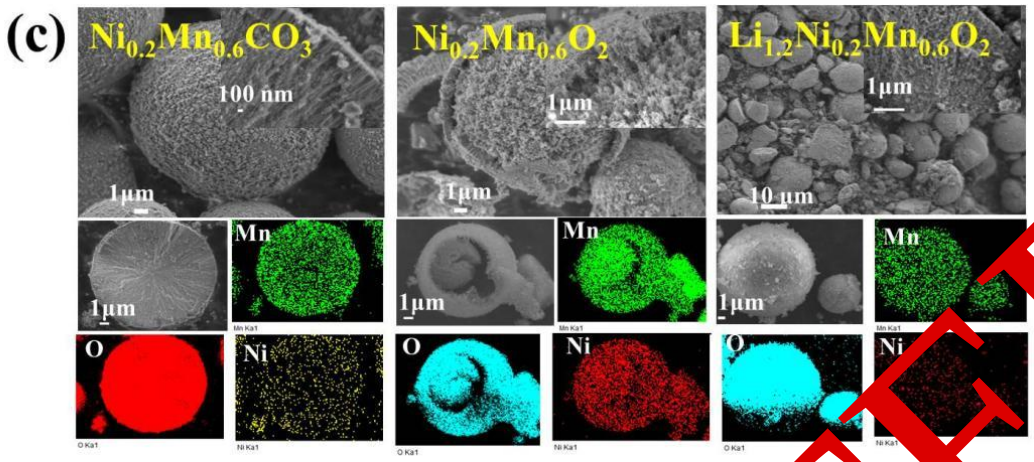

The phase transition in the circulation

The most important result of this work shows in Figure 3a. LNMO was assembled into the cell as the cathode material and tested *in-situ* DEMS. From the open circuit voltage 3.1 V to the charging voltage 4.8 V, there is no oxygen produced at all, which is an essential difference from the traditional LMR [11]. Furthermore, the oxygen precipitation peaks of 4.5 V disappear in Figure 3a and 2c, different from all the CV curves of traditional LMR. This means that the traditional phase transition mechanism has changed in this material LNMO. The structure of the material has changed dramatically too in Figure 3b. As the circulation progresses, it can be seen that the Li_2MnO_3 phase with the characteristic diffraction peak at about 21°is gradually disappearing and the spinel phase $LiMn_2O_4$ appears gradually, which indicates that Ni ions in $LiNi_{0.5}Mn_{1.5}O_4$ have come off. The corresponding situation occurs in Figure 3d, the voltage plateau represented for the oxidation of Ni ions at 4.73 V is gradually getting shorter, which is completely disappear after around 10 cycles. Compared the REDOX peak of Figure 3c with the voltage platform of Figure 3d, the platform of layered compound $LiMO_2$ is becoming and more obvious in the circulation of real cell. This also corresponds to the phenomenon that the discharge capacity is higher and higher because the theoretical specific capacity (237 mAh g^{-1}) of layered compounds is higher than that of the spinel phase (140 mAh g^{-1}).

Figure 3. (a) *In-situ* DEMS of LNMO cell between 3.1 to 4.8 V at the scanning speed of 0.5 mV s^{-1}. (b) *Ex-situ* XRD of LNMO in the circulation. (c) CV curves of LNMO between 2-4.8 V at the scanning speed of 0.3 mV s^{-1}. (d) the typical charge and discharge curves of LNMO. Note: (b) (•) R-3m, (•) C2/C, (•)Fd-3m, Fddd(•).

(c) 1st(—), 2nd(—), 3rd(—),4th(—),5th(—).

(d) 1st(—), 10th(—), 50th(—)

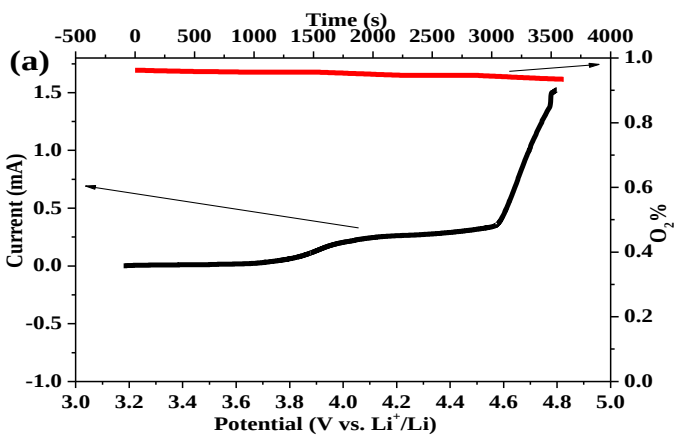

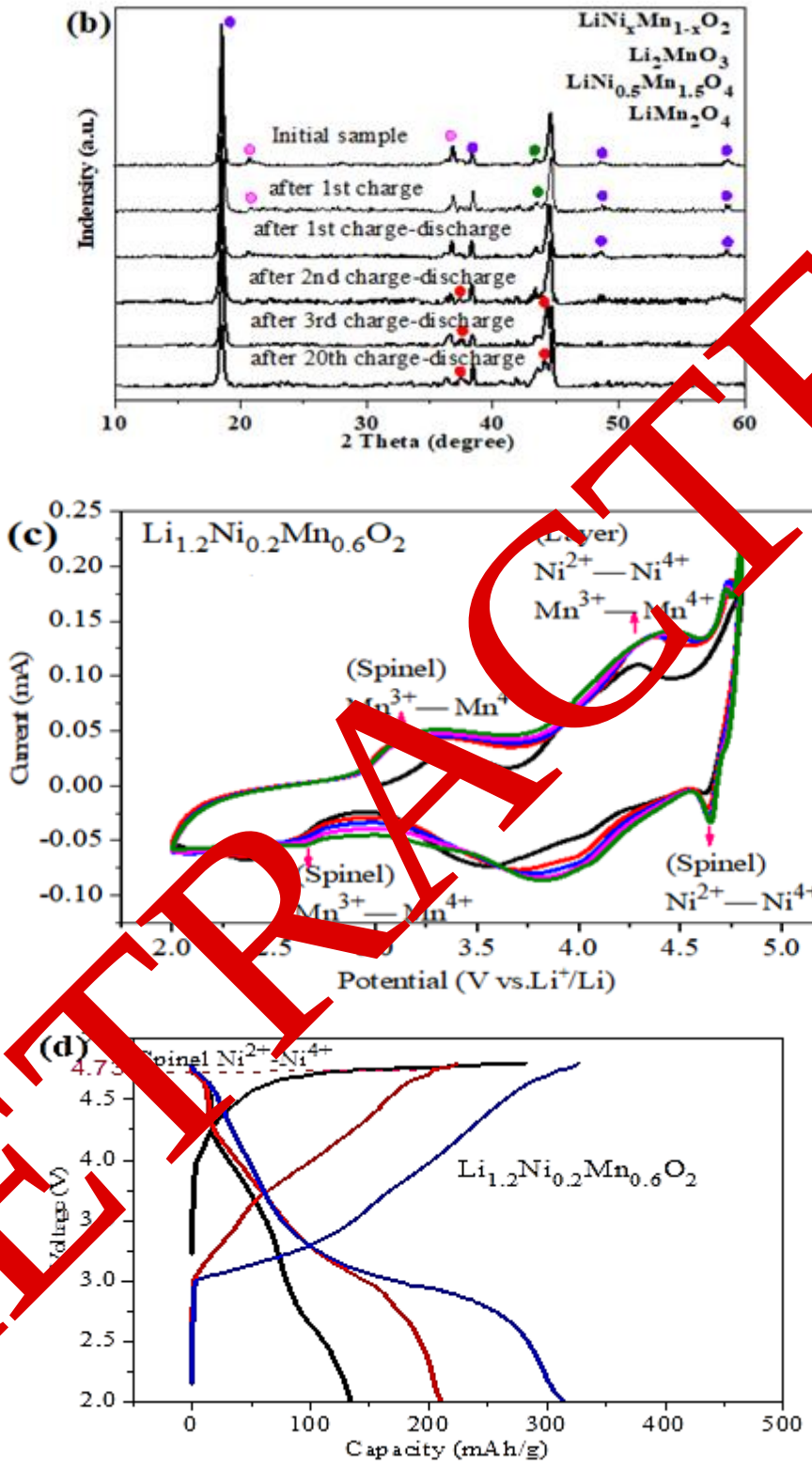

The above conclusions are further confirmed in Figure 3, which shows the HRTEM, SAED and EDS analysis of LNMO before and after 5 cycles. In the initial state, the material consists of three phases shown in SAED, lattice plane for $LiMO_2$, lattice plane for Li_2MnO_3 and lattice plane for $LiNi_{0.5}Mn_{1.5}O_4$. EDS analysis corresponding to $LiNi_{0.5}Mn_{1.5}O_4$ shows the auto ratio O: Mn: Ni is 12.85: 3.12: 0.9, which is similar to the theoretical ratio 4:1.5:0.5. While after 5 cycles, $LiNi_{0.5}Mn_{1.5}O_4$ and $LiMO_2$ still exist except for Li_2MnO_3. And in contrast to the XRD result, $LiMn_2O_4$ also appears. There is a layer of amorphous phase on the edge of the crystalline phase, which is considered as the SEI film.

Figure 4. The HRTEM, SAED and EDS analysis of LNMO before and after 5 cycles.

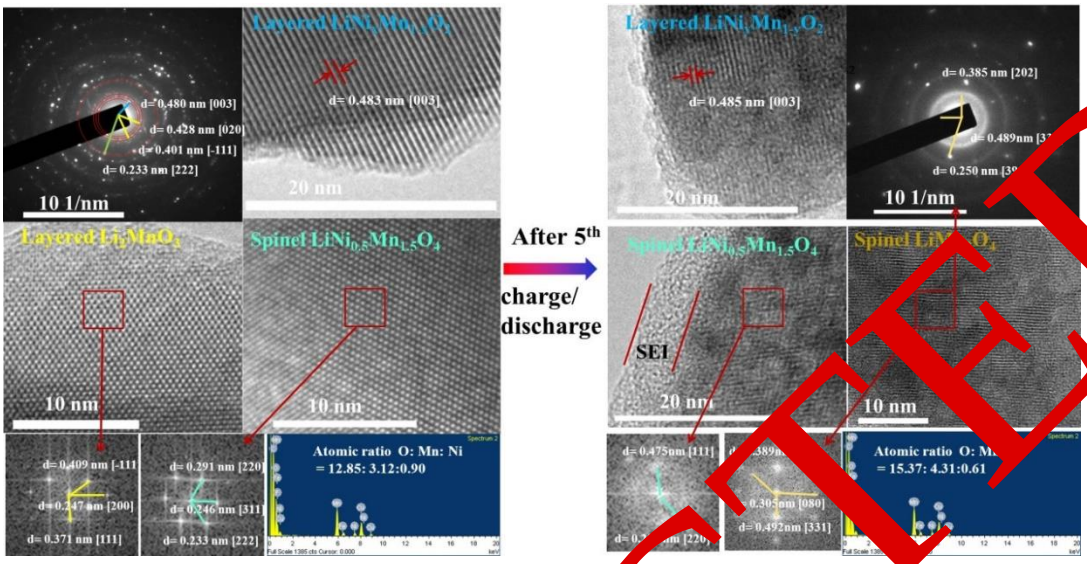

From the above phenomena, we can conclude that the Li_2MnO_3 is lost in the circulation, and Ni ions are gradually migrating out of spinel phase $LiNi_{0.5}Mn_{1.5}O_4$. The results of XPS give some clues to the transformation of LNMO. Ni-Mn bond intension in $LiNi_{0.5}Mn_{1.5}O_4$ is getting weak in Figure 4b, which means Ni-Mn bonds are getting fewer and fewer due to migration of Ni ions. From Figure 2c, the binding energy around 73 eV represent for MnO obviously enhance, which can be due to the reduction of Mn^{3+} in spinel phase $LiMn_2O_4$. The binding energy around 54.5 eV indicates Li^+ ions mainly exist in the Li-M layer of Li_2MnO_3 at the initial state, Li^+ ions in layered structure proportion increase after 5 cycles shown in Figure 4d, in which the binding energy was transferred to 55.5 eV. The result of the chemical state of oxygen confirms. The binding energy of oxygen at 528.5 eV denotes that oxygen is in the tetrahedron, while in the octahedron 531.5 eV. The oxygen is more in the tetrahedron of the spinel phase $LiNi_{0.5}Mn_{1.5}O_4$ and mo the octahedron of the layered structure $LiMO_2$ after 5 cycles shown in Figure 4e. In combination with the chang of chemical state of all elements, we have reason to believe that the Ni ions are migrating and the layered phase $LiMO_2$ increases in the circulation process.

Figure 4. The XPS analysis of LNMO for (a) NI_2P, (b) Ni LM_2-MN_2P, (c) MN_3S, (d) Li_1s, e O1s before and after 5 cycles. Note: As pr ared $Li_{1.2}Ni_{0.2}Mn_{0.6}O_2$ (———), $Li_{1.2}Ni_{0.2}Mn_{0.6}O_2$ After 5 Cycles (———).

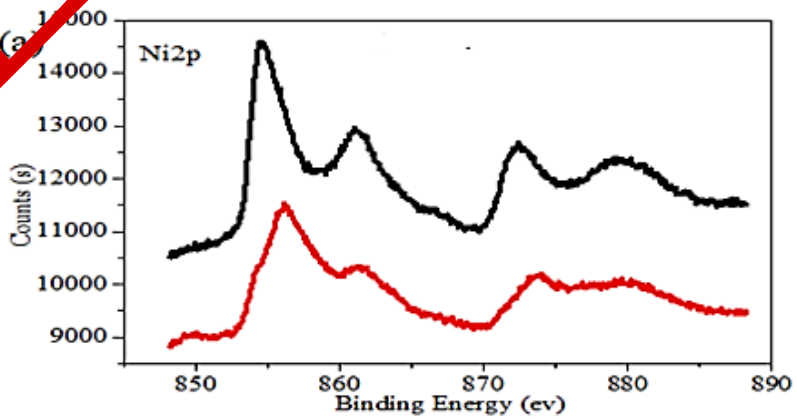

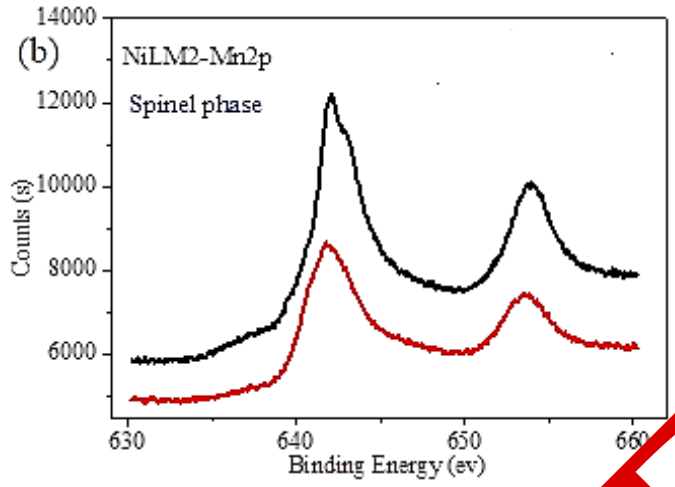
(b)
NiLM2-Mn2p
Spinel phase
Counts (s)
Binding Energy (ev)

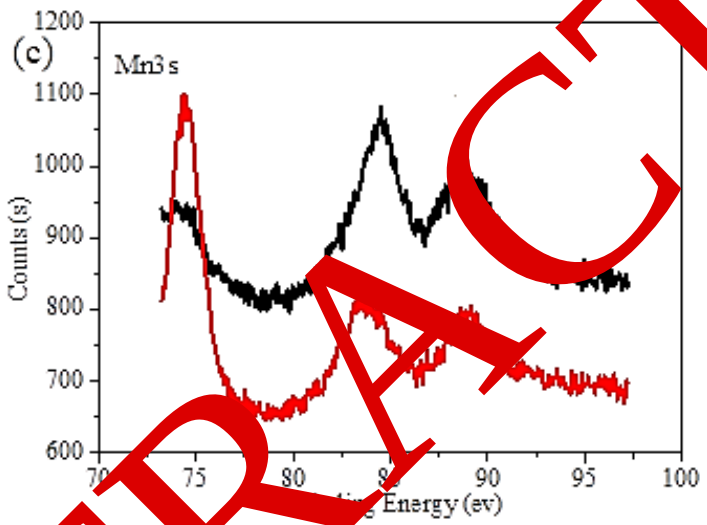
(c)
Mn3s
Counts (s)
Energy (ev)

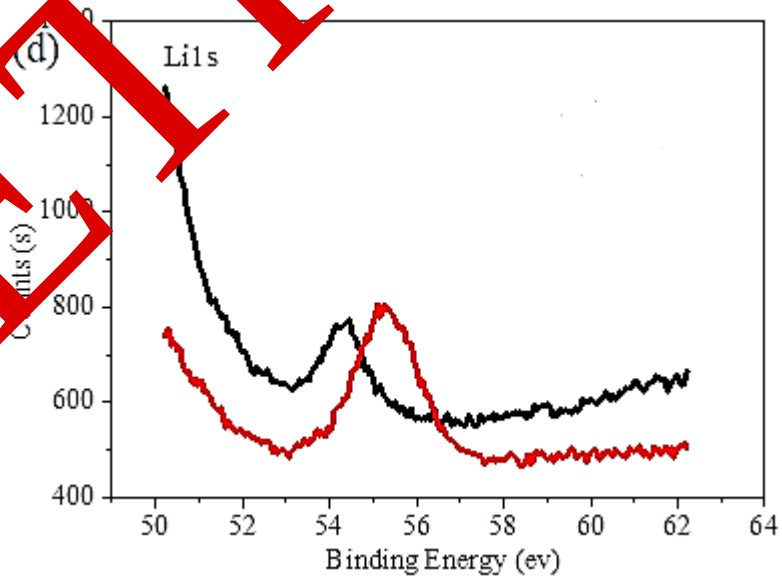
(d)
Li1s
Binding Energy (ev)

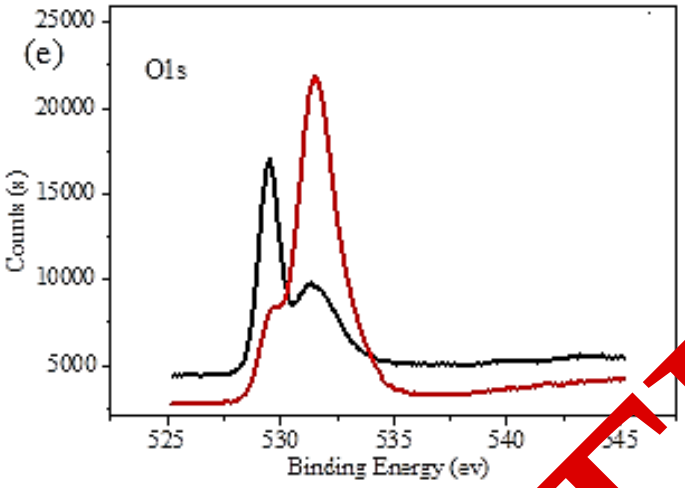

The electrochemical properties of $Li_{1.2}Ni_{0.2}Mn_{0.6}O_2$ for LIBs

Attributed to the change of lithium de-intercalation mechanism in the first cycle, LNMO did not lose oxygen, and the structure remained relatively stable for a long time. Therefore, the electrochemical performance of LNMO is stable and excellent. The cycling and rate performance of LNMO are shown in Figure 5 (a, b). The capacity of LNMO maintain 300 mAh/g at the rate of 0.1 C (25 mA g^{-1}) and 200 mAh g^{-1} at the rate of 0.5 C after 200 cycles. In the process of the initial cycles, the capacity shows an uptrend, which is the influence of transformation from Li_2MnO_3 to $LiMO_2$. After several cycles, the phase transition is completed, and the structure is relatively stable composed of layered $LiMO_2$ and spinel $LiMn_2O_4$ with no attenuation of the voltage platform and no decay of capacity. Figure 5b reveals good rate performance, from which the capacity of LNMO are 250, 220, 200, 150, 100, 50 mAh g^{-1} at the rate of 0.1, 0.2, 0.5, 1, 5,10 C, respectively. When the rate returns to 0.1 C, the capacity goes back to 250 mAh g^{-1}.

The Nyquist plots for LNMO derived from the EIS measurements without circulation and after 5th, 20th cycles are shown in Figure 5c. All the spectra exhibit a semicircle at high-medium frequencies corresponding to the charge transfer resistance (Rct). It is that rather different behavior in Rct is observed. As shown here, Rct increases from 86.4 to 200.1, 259.8 Ω, which means the surface electrode reaction is increasingly difficult as the circulation goes on. Inclined line in the low-frequency range is considered as the Warburg impedance, corresponding to the Li^+ diffusion inside the electrode material [32]. The numerical value of the Li^+ diffusion coefficient in the electrode can be estimated from the following equation [32].

$$D_{Li^+} = 0.5[\frac{V_m}{FSA_w}(-\frac{dE}{dx})]^2$$

Figure 5d shows the trend that the slope represents Warburg coefficients (A_w) increases with circulation, which is belong to the change of crystal structure. The Warburg coefficients (A_w) of the cells with circulation and after 5,20 cycles are 1454.9, 2040.3, 2375.9 $\Omega/\omega^{-1/2}$, respectively. These results are consistent with the above electrochemical properties of LNMO.

Figure5. (a) The cycle performance of LNMO at the rate of 0.1C and 0.5C (b) The rate performance of LNMO (c) Electrochemical impedance spectra (EIS) of LNMO. (d) Linear fitting of Warburg impedance of LNMO. Note:

(a) Charge ( ), Discharge ( ), Charge( ), Discharge ( ), (b) Charge ( ), Discharge ( ), (c) Without circulation ( ), 5th ( ),20th ( ), (d) Without circulation ( ), 5th ( ), 20th ( ),

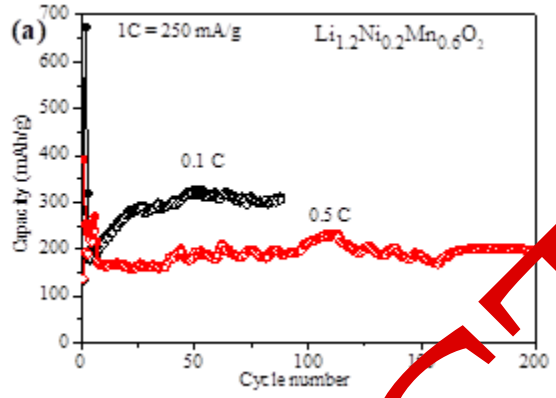

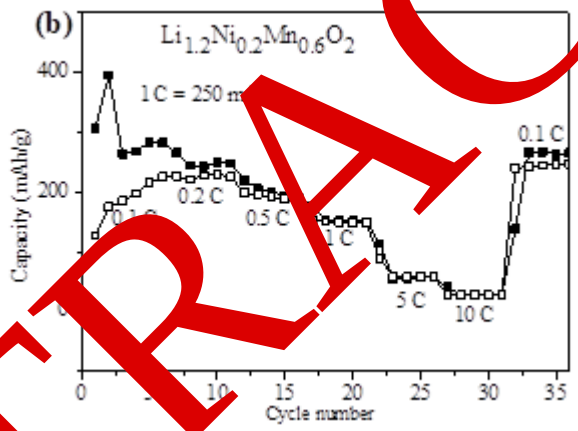

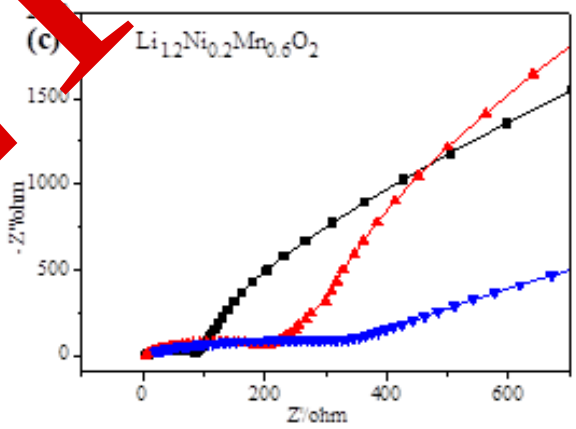

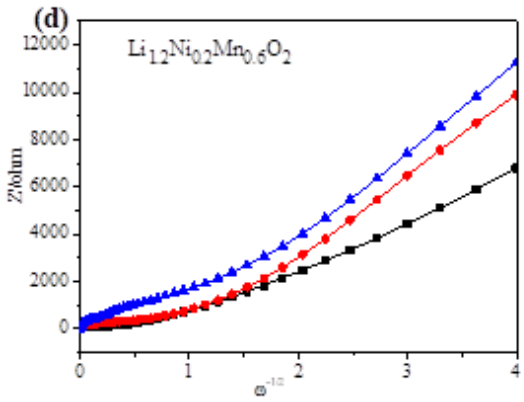

CONCLUSION

In this work, the lithium-rich manganese-based cathode material LNMO was synthesized by hydrothermal-annealing method. X-ray diffraction measurements shows the synthesized LNMO was composed of $LiMO_2$ and Li_2MnO_3 with layered structure and $LiNi_{0.5}Mn_{1.5}O_4$ with spinel structure. In the initial cycling process of general lithium-rich manganese-based materials, due to the irreversible transformation of the layered structure of Li_2MnO_3 into MnO_2, Li^+ and oxygen, a large amount of oxygen will escape, which will cause side reactions to lead to the deterioration of the electrolyte and the serious attenuation of battery capacity. CV curves of the as-prepared LNMO have no oxygen evolution peak and no oxygen appears *in situ* Differential Electrochemical Mass Spectrometry (DEMS) [50]. According to the first principle, Li^+ ions in Li_2MnO_3 de-intercalate when Ni^{2+} ions of $LiNi_{0.5}Mn_{1.5}O_4$ migrate into the sites when first charging, which avoids the oxygen loss from the collapse of Li_2MnO_3. The exist of spinel phase make the phase transition process of circulation stable, which contributed to the high cycling performance for lithium-ion battery (300 and 220 mAh g^{-1} after 200th cycles at 0.1 and 0.5C-rate (1C= 250 mA g^{-1}).

ACKNOWLEDGEMENTS

The authors acknowledge financial support from the Key Program of the Chinese Academy of Sciences (Grant No. KGZD-EW-T08).

REFERENCES

1. Qiu B, et al. Enhanced electrochemical performance with surface coating by reactive magnetron sputtering on lithium-rich layered oxide electrodes. ACS Appl. Mater. Interfaces. 2014;6: 9187−9193.
2. Liu HJ, et al. High-energy 'composite' layered manganese-rich cathode materials *via* controlling Li_2MnO_3 phase activation for lithium-ion batteries. Phys. Chem. Chem. Phys. 2012;14: 6584-6595.
3. Qiu B, et al. Effects of Na^+ contents on electrochemical properties of $Li_{1.2}Ni_{0.13}Co_{0.13}Mn_{0.5402}$ cathode materials. J. Power Sources. 2013;240: 530−535.
4. Wang J, et al. Electrochemical properties of 0.6Li[Li1/3Mn2/3]02−0.4LiNixMnyCo1−x−y02 cathode materials for lithium-ion batteries. J.Power Sources. 2012;218:128-133.
5. Qiu S, et al. Synthesis of monoclinic $Li[Li_{0.2}Mn_{0.54}Ni_{0.13}CO_{0.13}]O_2$ nanoparticles by a layered-template route for high-performance li-ion batteries. Eur. J. Inorg. Chem. 2013;16:2887−2892.
6. Zhao CH, et al. Mn-Ni content-dependent structures and electrochemical behaviors of serial $Li_{1.2}Ni_{0.13}$+ x $co_{0.13}Mn_{0.54-x}O_2$ as lithium-ion battery cathodes. ACS Appl. Mater. Interfaces. 2014;6: 2386−2392.

7. Jiang KC, et al. Superior hybrid cathode material containing lithium-excess layered material and graphene for lithium-ion batteries. ACS Appl. Mater. Interfaces 2012;4:4858-4863.
8. Shunmugasundaram R, et al. High capacity li-rich positive electrode materials with reduced first-cycle irreversible capacity loss. Chem. Mater. 2015;27: 757−767.
9. Riekehr L, et al. Effect of pristine nanostructure on first cycle electrochemical characteristics of lithium-rich lithium-nickel-cobalt-manganese-oxide cathode ceramics for lithium ion batteries. J.Power Sources. 2016;306:135-147.
10. Armstrong AR, et al. Demonstrating oxygen loss and associated structural reorganization in the lithium battery cathode $Li[Ni_{0.2}li_{0.2}Mn_{0.6}]o_2$. J. Am. Chem. Soc. 2006;128:8694-8698.
11. Grey CP, et al. Electrochemical activity of li in the transition-metal sites of o3 $Li\,[Li_{(1-2x)/3}Mn_{(2-x)/3}Ni_x]\,O_2$. Electrochem. Solid-State Lett. 2004;7: A290-A293.
12. Xu, B, et al. Identifying surface structural changes in layered Li-excess nickel manganeseoxides in high voltage lithium ion batteries: A joint experimental and theoretical study. Energy Environ. Sci. 2011;4:2223-2233.
13. Luo K, et al. Anion redox chemistry in the cobalt free 3d transition metal oxide intercalation electrode $Li[Li_{0.2}Ni_{0.2}Mn_{0.6}]O_2$. J. Am. Chem. Soc. 2016;138:11211-11218.
14. Zheng JM, et al. Structural and chemical evolution of Li- and Mn-rich layered cathode material. Chem. Mater. 2015;27:1381-1390.
15. Zheng JM, et al. Corrosion/Fragmentation of layered composite cathode and related capacity/voltage fading during cycling process. Nano Lett. 2013;13: 3824-3830.
16. Lu P, et al. Observation of electron-beam-induced phase evolution mimicking the effect of the charge–discharge cycle in Li-rich layered cathode materials used for Li ion batteries. Chem. Mater. 2015;27:1375-1380.
17. Xiao P, et al. Calculation of oxygen stability in lithium-rich layered cathodes. J. Phys. Chem. C. 2012;116:23201−23204.
18. Kim MG, et al. Template-free synthesis of $Li[Ni_{0.25}Li_{0.15}Mn_{0.6}]O_2$nanowires for high performance lithium battery cathode. Chem. Commun. 2009;218–220.
19. Chen J, et al. Synthesis and characterization of $Li[NI_{0.41}Li_{0.08}MN_{0.51}]O_2$ nanoplates for li battery cathode material. J. Phys. Chem. C. 2007;111:3192-3196.
20. Yao K, et al. One-pot synthesis of lithium-rich cathode material with hierarchical morphology. Nano Lett. 2016;16:7503-7508.
21. Feng Wu, et al. Spinel/layered heterostructured cathode material for high-capacity and high-rate Li-ion batteries. Adv. Mater. 2013, 25, 3722-3726.
22. Liu JT, et al. The effect of boron doping on structure and electrochemical performance of lithium-rich layered oxide materials. ACS Appl. Mater. Interfaces 2016;8: 18008-18017.
23. Jin X, et al. Improvement in rate capability of lithium-rich cathode material $Li[Li_{0.2}Ni_{0.13}Co_{0.13}Mn_{0.54}]O_2$ by Mo substitution. Ionics 2016;22:1369-1376.
24. Chen S, et al. Synergistic effects of stabilizing the surface structure and lowering the interface resistance in improving the low-temperature performances of layered lithium-rich. ACS Appl. Mater. Interfaces. 2017;9: 8641-8648.
25. Bian XF, et al. Multi-functional surface engineering for li-excess layered cathode material targeting excellent electrochemical and thermal safety properties. ACS Appl. Mater. Interfaces

2016;8:3308-3318.

26. Zhang J, et al. Polyimide encapsulated lithium-rich cathode material for high voltage lithium-ion battery. ACS Appl. Mater. Interfaces 2014;6:17965-17973.
27. Song BH, et al. Long-life nickel-rich layered oxide cathodes with a uniform LI_2ZRO_3 surface coating for lithium-ion batteries. ACS Appl. Mater. Interfaces. 2017;9:9718-9725.
28. Wu F, et al. Surface modification of li-rich cathode materials for lithium-ion batteries with a pedot:Pss conducting polymer. ACS Appl. Mater. Interfaces 2016;8: 23045-23054.
29. Guo LC, et al. Surface double phase network modified lithium rich layered oxides with improved rate capability for Li-ion batteries. ACS Appl. Mater. Interfaces, 2015;7:391-3
30. Zheng JM, et al. Functioning mechanism of ALF_3 coating on the and MN-Rich cathode materials. Chem. Mater. 2014;26:6320-6327.
31. Bloom I, et al. Effect of interface modifications on voltage fade in Li_2Mn $LiNi_{0.375}Mn_{0.375}CO_{0.2502}$ cathode materials. J. Power Sources. 2014;249 509-514.
32. Wu F, et al. Multifunctional alpo4 coating for improving electrochemical properties of low-cost $Li[Ii_{0.2}Fe_{0.1}Ni_{0.15}Mn_{0.55}]O_2$ cathode materials for ium-ion batteries. ACS Appl. Mater. Interfaces 2015;7:3773-3781.
33. Guo L,Li JJ,Cao TT, Wang HY, Zhao JQ, H (2016) ACS Appl. Mater. Interfaces 8: 24594−24602.
34. Gu M, et al. Formation of the spinel phase in the layered composite cathode used in Li-ion batteries. ACS NANO. 2013, 760-767.
35. Jin YC, et al. Fluorin ion Inh the surface segregation of high voltage spinel on Lithium-rich layered cathodes for enhanced rate capability in lithium ion batteries. ACS Appl. Mater. Interfaces 2016; 83-3891.
36. Chen M, et al. ayered Lithium-rich oxide nanoparticles doped with spinel phase: Acidic sucrose-assistant synthesis and excellent performance as cathode of lithium ion battery. ACS Appl. Mater. Interfaces. 2016;8: 4575-4584.
37. Wu F, et al. Ultrathin spinel membrane-encapsulated layered lithium-rich cathode material for advanced Li-ion batteries. Nano Lett. 2014;14:3550-3555.
38. Chen S, et al. Enhanced electrochemical performance of layered Lithium-rich cathode materials by constructing spinel-structure skin and Ferric Oxide islands. ACS Appl. Mater. Interfaces. 2017;9:8669-8678.
39. Yu HJ, et al. High-energy cathode materials (Li_2MnO_3-$LiMO_{2)}$ for lithium-ion batteries. J. Phys. Chem. Lett. 2013;4:1268-1280.
40. Chen YF, et al. The significance of the stable Rhombohedral structure in Li-rich cathodes for lithium-ion batteries. Ionics. 2017;23:367–375.
41. Zheng JM, et al. Mitigating voltage fade in cathode materials by improving the atomic level uniformity of elemental distribution. Nano Lett. 2014;14:2628-2635.
42. Jung YS, et al. Effects of atomic layer deposition of AL_2O_3 on the Li $[LI_{0.20}MN_{0.54}Ni_{0.13}CO_{0.13}]O_2$ cathode for lithium-ion batteries. J. Electrochem. Soc. 2011;158: A1298−A1302.
43. Scott ID, et al. Ultrathin coatings on nano-$LiCOO_2$ for li-ion vehicular applications. Nano Lett. 2011;11:414-418.

44. Zhao JQ, et al. Ultrathin surface coatings for improved electrochemical performance of lithium ion battery electrodes at elevated temperature. J. Phys. Chem. C 2012;116:11867-11876.
45. Liu J, et al. Conductive surface modification with aluminum of high capacity layered $Li[Li_{0.2}Mn_{0.54}Ni_{0.13}Co_{0.13}]O_2$ Cathodes. J. Phys. Chem. C. 2010;114: 9528-9533.
46. Liu J, et al. Carbon-coated high capacity layered $Li[Li_{0.2}Mn_{0.54}Ni_{0.13}Co_{0.13}]O_2$ cathodes. Electrochem. Commun. 2010;12:750-753.
47. Shin DW, et al. ZrO_2-modified $LiMN_2O_4$ thin-film cathodes prepared by pulsed laser deposition. J. Electrochem. Soc. 2010;157:A567-A570.
48. Hong RJ, et al. Influence of oxygen partial pressure on the structure and photoluminescence of direct current reactive magnetron sputtering ZnO thin films. (2005) Thin Solid Films 473:58-62.
49. Li L, et al. X-ray photoelectron spectroscopy study and thermoelectric properties of Al-doped ZnO thin films. Electron. Spectrosc. Relat. Phenom. 2009;173: 7-11.
50. Ellmer KJ. Magnetron sputtering of transparent conductive zinc oxide: Relation between the sputtering parameters and the electronic properties. Phys. D: Appl. Phys. 2000;33: R17.